Phase correction of Gabor deconvolution

Tianci Cui and Gary F. Margrave

ABSTRACT

Seismic data is always nonstationary due to ubiquitous anelastic attenuation modeled by the constant-Q theory. The stationary spiking deconvolution of stationary traces is extended to Gabor deconvolution of nonstationary traces, in which a seismic trace is decomposed into a time-frequency spectrum by the windowed Fourier transform and a nonstationary wavelet is estimated within each window. The amplitude spectrum of the nonstationary wavelet is accurately estimated by a smoothing process while its phase spectrum is calculated by the discrete Hilbert transform integrating within the seismic frequency band only. The Gabor deconvolved seismic trace ties the well reflectivity in amplitude and spectral content, but has phase being corrected respect to the seismic Nyquist frequency only. The phase error is the phase difference of the nonstationary wavelet with respect to the well logging frequency and the seismic Nyquist frequency. It can be calculated by knowing the Q values and the well logging frequency, to serve as a phase correction operator in the Gabor domain, which is equivalent to a time-variant residual drift time correction operator in the time domain. Without knowledge of Q or the well logging frequency, the residual drift time can be estimated by smooth dynamic time warping, which is more accurate than that estimated by time-variant crosscorrelation. The Gabor deconvolved nonstationary trace with phase or residual drift time correction ties the well reflectivity with little amplitude or phase errors.

GABOR TRANSFORM

Margrave and Lamoureux (2001) extends the stationary deconvolution theory to the nonstationary case using the Gabor transform, which is essentially a windowed Fourier transform. The forward Gabor transform decomposes a 1-D temporal signal $s(t)$ onto a 2-D time-frequency spectrum by windowing the signal with a set of Gaussian functions summing to unity and Fourier transforming:

$$\hat{s}_g(\tau, f) = \int_{-\infty}^{\infty} s(t) g_\sigma(t-\tau) e^{-2\pi i f t}\, dt \tag{1}$$

where $g_\sigma(t-\tau)$ is a Gaussian function of standard width 2σ centered at time τ and $\hat{s}_g(\tau, f)$ is the complex-valued Gabor spectrum of $s(t)$. Given $\hat{s}_g(\tau, f)$, the inverse Gabor transform recreates the signal via 2-D integration over the time-frequency plane:

$$s(t) = \int_{-\infty}^{\infty} \int_{-\infty}^{\infty} \hat{s}_g(\tau, f) e^{2\pi i f t}\, df\, d\tau. \tag{2}$$

Figure 1 shows the forward Gabor transform of the nonstationary trace using a set of Gaussian windows with 100 ms half-width (σ) and 10 ms increment, every 10^{th} of which is plotted in the middle panel. The right panel is the magnitude of its Gabor spectrum, showing that the nonstationary trace contains the greatest power at early times and low

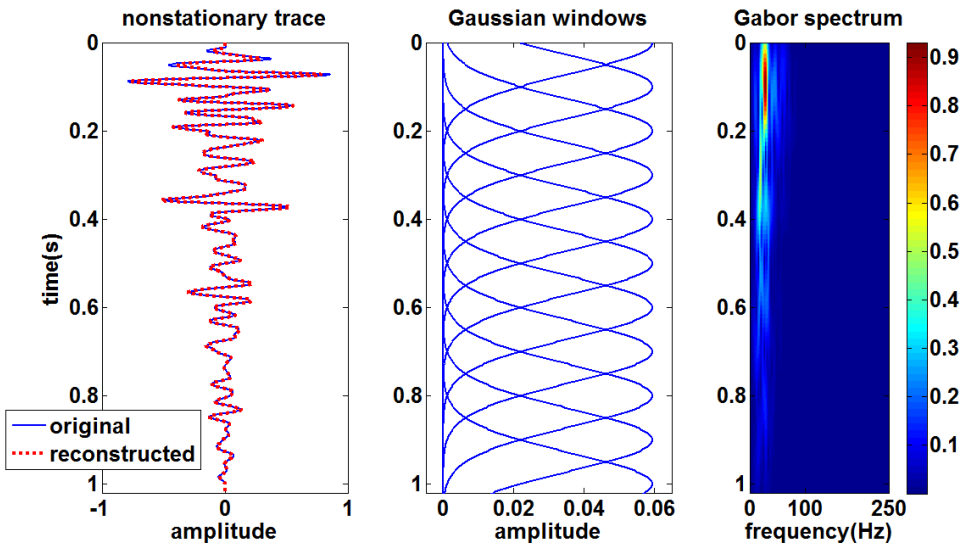

FIG. 1. The forward and inverse Gabor transform is demonstrated. The nonstationary trace after forward and inverse Gabor transform is on top of the original trace (left). A set of selected Gaussian windows used for the forward Gabor transform (middle). The Gabor magnitude spectrum of the nonstationary trace (right).

frequencies and the rapid fluctuations are attributed to the reflectivity. The inverse Gabor transform of the 2-D spectrum reconstructs the nonstationary trace, which is consistent with the original one shown in the left panel.

Margrave and Lamoureux (2001) derived that the Gabor transform of the nonstationary convolutional model (Margrave, 1998) can be approximated as

$$\hat{s}_g(\tau, f) \approx \hat{w_0}(f)\alpha(\tau, f)\hat{r}_g(\tau, f) \tag{3}$$

where $\hat{w_0}(f)$ is the Fourier transform of the source wavelet $w_0(t)$ and $\hat{r}_g(\tau, f)$ is the Gabor transform of the reflectivity $r(t)$. The Fourier transform of the propagating wavelet is

$$\hat{w_Q}(\tau, f) = \hat{w_0}(f)\alpha(\tau, f). \tag{4}$$

Therefore, Equation 3 can also be written as

$$\hat{s}_g(\tau, f) \approx \hat{w_Q}(f)\hat{r}_g(\tau, f). \tag{5}$$

Equation 5 shows that that within a single Gaussian window which is centered at time τ and is narrow enough, the stationary convolutional model that the seismic trace can be modeled by the stationary convolution of a seismic wavelet with the reflectivity (Sheriff and Geldart, 1995) is locally valid. Thus, in the frequency domain, the windowed trace is the product of the nonstationary wavelet propagating to time τ and the windowed reflectivity. Figure

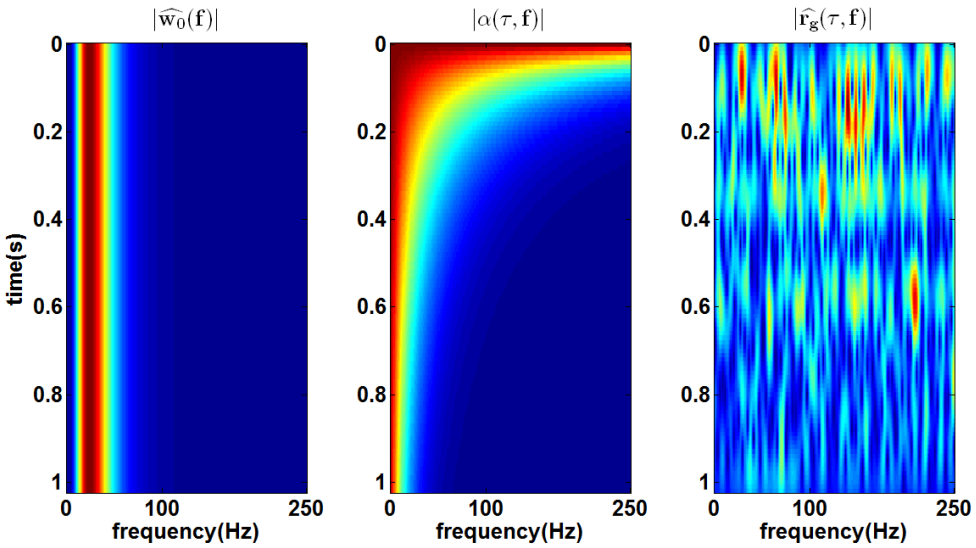

FIG. 2. The magnitude of three components: the Fourier transform of the source wavelet duplicated along the traveltime (left), the attenuation function represented on the time-frequency plane (middle) and the Gabor spectrum of the reflectivity (right).

2 displays the magnitude of each component on the right hand side of Equation 3. The source wavelet is a time-invariant function. The attenuation function consists of seamless hyperbolic trajectories with the time and frequency axes as asymptotes. The reflectivity varies rapidly in both time and frequency. Figure 3 left panel is the pointwise product of those three components and it well approximates the Gabor magnitude spectrum of the nonstationary trace shown in Figure 3 right panel, validating the nonstationary convolutional model factorization in the Gabor domain. Figure 4 left panel shows the pointwise product of the Gabor magnitude spectra of the source wavelet and the attenuation function to form the Gabor magnitude spectrum of the propagating wavelet by Equation 4.

GABOR DECONVOLUTION

In analogy with the stationary deconvolution, estimating $\hat{r}_g(\tau, f)$ needs the spectral factorization of $\hat{s}_g(\tau, f)$ into two unknown parts: the propagating wavelet and the reflectivity. This can be solved based on the fact that $|\hat{w_Q}(\tau, f)|$ is relatively smooth compared to the rapidly varying $\hat{r}_g(\tau, f)$. Thus, they can be estimated by a spectral smoothing process without knowing or estimating Q values. Similar to the stationary deconvolution, the wavelet design portion of Gabor deconvolution works on the amplitude spectra only and determines the wavelet phase spectrum based on the minimum-phase assumption. Take the absolute values of Equation 5:

$$|\hat{s}_g(\tau, f)| \approx |\hat{w_Q}(\tau, f)||\hat{r}_g(\tau, f)|. \tag{6}$$

The simplest Gabor deconvolution algorithm estimates $|\hat{w_Q}(\tau, f)|$ by smoothing $|\hat{s}_g(\tau, f)|$ via convolving it with a 2-D boxcar over τ and f

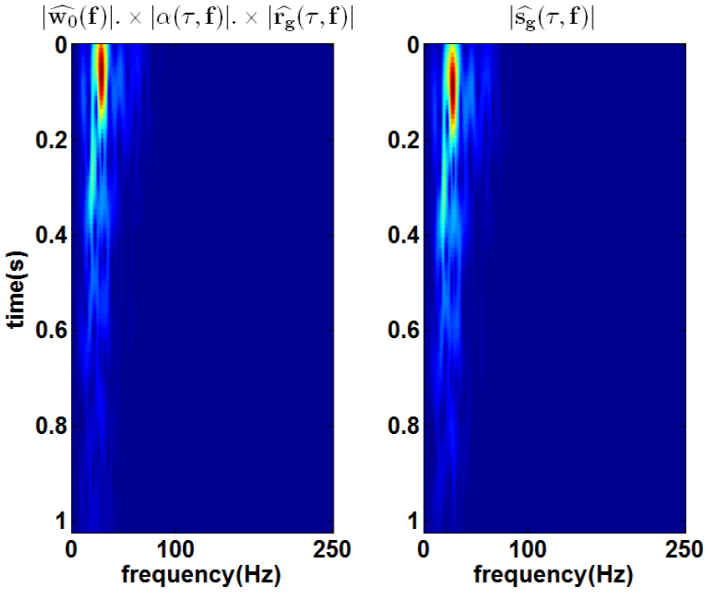

FIG. 3. The pointwise product of the three magnitude spectra in Figure 2 (left) and the Gabor magnitude spectrum of the nonstationary trace (right), which is the same as Figure 1 right panel.

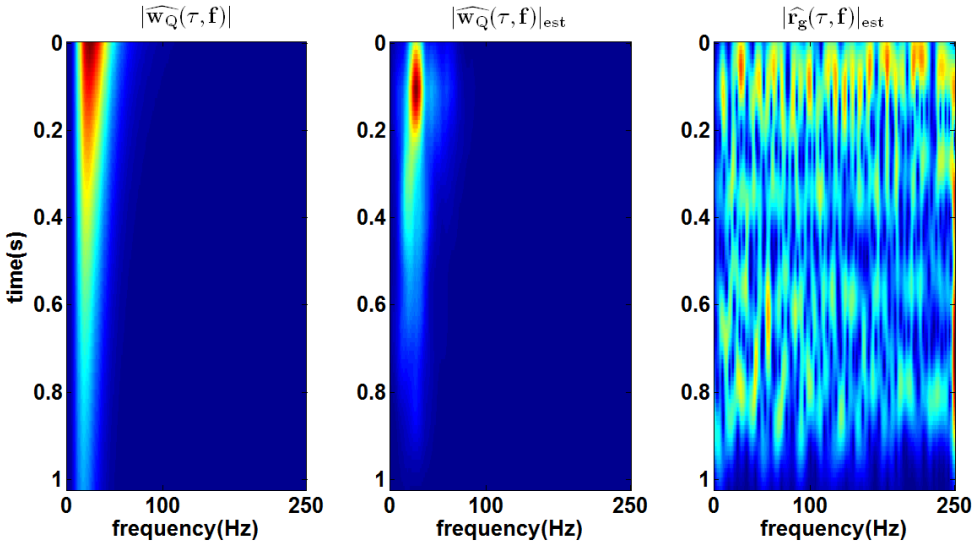

FIG. 4. The Gabor magnitude spectra of the propagating wavelet (left), the estimated propagating wavelet (middle) and the estimated reflectivity (right) by Gabor deconvolution.

$$|\hat{w_Q}(\tau, f)|_{est} = \overline{|\hat{s}_g(\tau, f)|}. \tag{7}$$

Since both the source wavelet and the attenuation function are assumed to be minimum-phase, the phase of the nonstationary wavelet $\phi_{w_Q}(\tau, f)$ at a constant time τ is also minimum and is calculated by the Hilbert transform

$$\phi_{w_Q}(\tau, f) = -\frac{1}{\pi} \int_{-\infty}^{\infty} \frac{\ln |\hat{w_Q}(\tau, \tilde{f})|_{est}}{f - \tilde{f}} d\tilde{f}. \tag{8}$$

In the digital implementation, the integral must be calculated within the seismic frequency band only

$$\phi_{w_Q}(\tau, f) = -\frac{1}{\pi} \int_{-f_{NYQ}}^{f_{NYQ}} \frac{\ln |\hat{w_Q}(\tau, \tilde{f})|_{est}}{f - \tilde{f}} d\tilde{f}. \tag{9}$$

Next $\hat{r}_g(\tau, f)$ is estimated by dividing $\hat{w_Q}(\tau, f)_{est}$ from $\hat{s}_g(\tau, f)$ and $r_{est}(t)$ is got by inverse Gabor transforming $\hat{r}_g(\tau, f)_{est}$.

Figure 4 middle panel shows the Gabor magnitude spectrum of the estimated propagating wavelet by convolving the Gabor magnitude spectrum of the nonstationary trace in Figure 3 right panel with a 2-D boxcar of dimensions 0.2 s by 10 Hz. The estimate approximates the known propagating wavelet in Figure 4 left panel. Figure 4 right panel shows the Gabor magnitude spectrum of the estimated reflectivity by pointwise division of Figure 4 middle panel from Figure 3 right panel. It approximates the known reflectivity in Figure 2 right panel to achieve a strong broadband whitening.

After the inverse Gabor transform, the nonstationary trace after Gabor deconvolution is shown in the time domain as the green curve in Figure 5. There is no such nonstationary catastrophe (Margrave, 2013) as running stationary deconvolution on the nonstationary trace and the reflectivity is well resolved. The amplitude spectra of its three sections are plotted in Figure 6, showing the appropriate whitening of all the sections. Next, the amplitude of the Gabor deconvolved trace is balanced and its phase is rotated with respect to the known reflectivity in the same time-variant way as the well tying procedure by the stationary deconvolution. In this case, the time-variant amplitude balancing changes little of the deconvolved trace because the smoothing process does a kind of AGC (automatic gain correction) and simultaneously gains the trace in time. Figure 5 shows the final estimate in red on top of the known reflectivity in blue. It can be observed that they roughly tie in amplitude and spectral content but not the phase and/or timing. The time-variant constant-phase differences, crosscorrelation coefficient sequences and time shift sequences are also shown in Figure 7 as a quality control. It can be seen that the results at every well-tying step are similar to the case of running the stationary deconvolution. In conclusion, running Gabor deconvolution on the nonstationary trace can get reflectivity estimate tying the well reflectivity in amplitude and spectral content, but has phase errors which are more complex than those can be solved by time-variant constant-phase rotation.

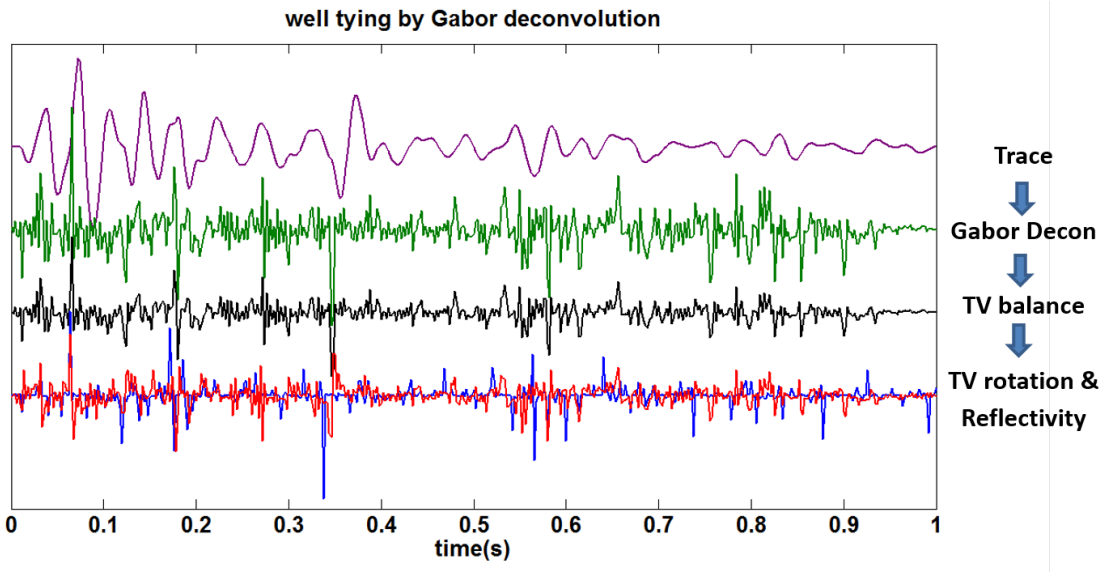

FIG. 5. A procedure of tying the nonstationary trace to the known reflectivity (blue) by Gabor deconvolution, time-variant amplitude balancing and time-variant constant-phase rotation.

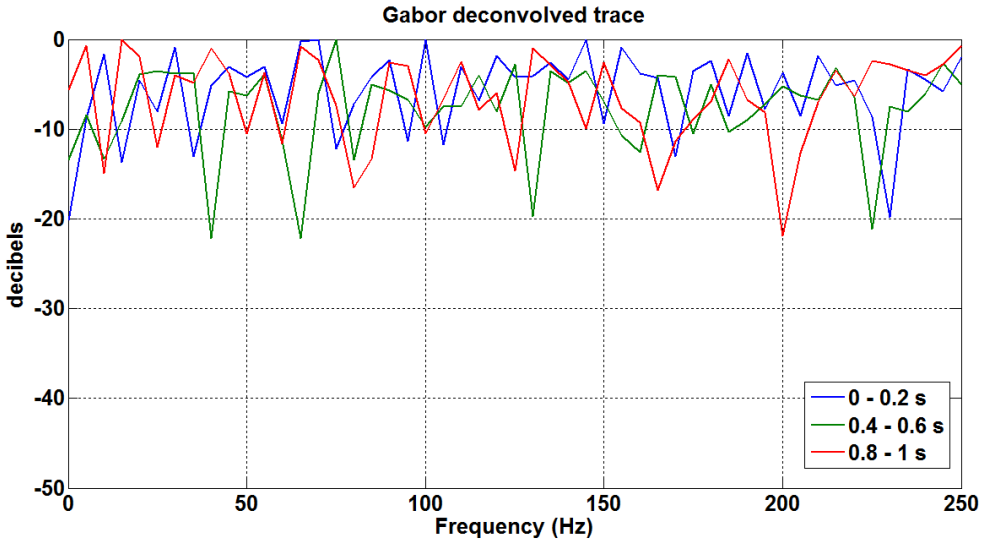

FIG. 6. Amplitude spectra of the Gabor deconvolved seismic trace within different time ranges in decibels.

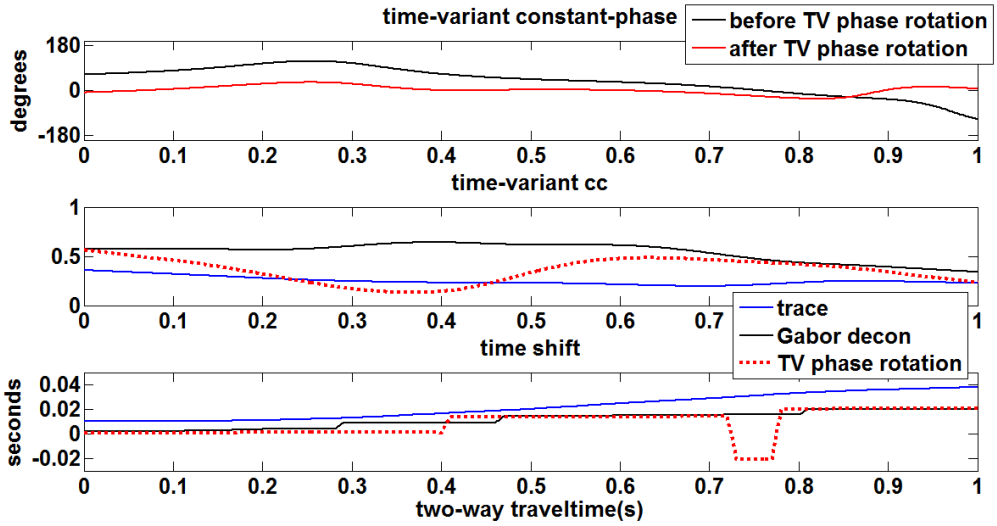

FIG. 7. The time-variant constant-phase differences between the known reflectivity and the Gabor deconvolved trace before and after phase rotation (top). The time-variant crosscorrelation coefficient sequences between the known reflectivity and the nonstationary trace, the Gabor deconvolved trace after time-variant amplitude balancing, the Gabor deconvolved trace after time-variant amplitude balancing and time-variant constant-phase rotation (middle). The time-variant time shift sequences at which the coefficients are obtained (bottom).

PHASE CORRECTION OF GABOR DECONVOLUTION

To find out the reason for the residual phase after Gabor deconvolution, the propagating wavelets estimated by Gabor deconvolution are investigated. Figure 8 shows the estimated wavelets propagating to every 0.1 s in black, on top of which are the corresponding wavelets embedded in the nonstationary trace in red. Since the spectral separation of the propagating wavelets from the reflectivity is only determined to within a scale factor, the estimated wavelets are overall scaled so that the maximum amplitude of the estimated wavelet at time zero is equal to that of the known source wavelet for easy comparison. It can be observed that the estimated wavelets have the correct relative amplitudes and waveforms (except for those at early times suffering from the edge effects), but they appear progressively earlier than the Q wavelets. Both the estimated and known wavelets propagating to four times: 0.3 s, 0.4 s, 0.5 s and 0.6 s are further studied in the frequency domain. Figure 9 compares their normalized amplitude spectra, verifying that the smoothing process in Gabor deconvolution estimates accurate amplitude spectra of the propagating wavelets. Figure 10 compares their unwrapped phase spectra after their propagating times at the high frequency reference velocity v_0 being removed. It can be seen that the phase estimated by Gabor deconvolution is insufficient compared to the Q wavelets.

The phase estimation errors result from the fact that the bandlimited Hilbert transform must be used (Equation 9) instead of the analytic one (Equation 8). The calculated phase is essentially with respect to the seismic Nyquist frequency f_{NYQ} (Margrave et al., 2011)

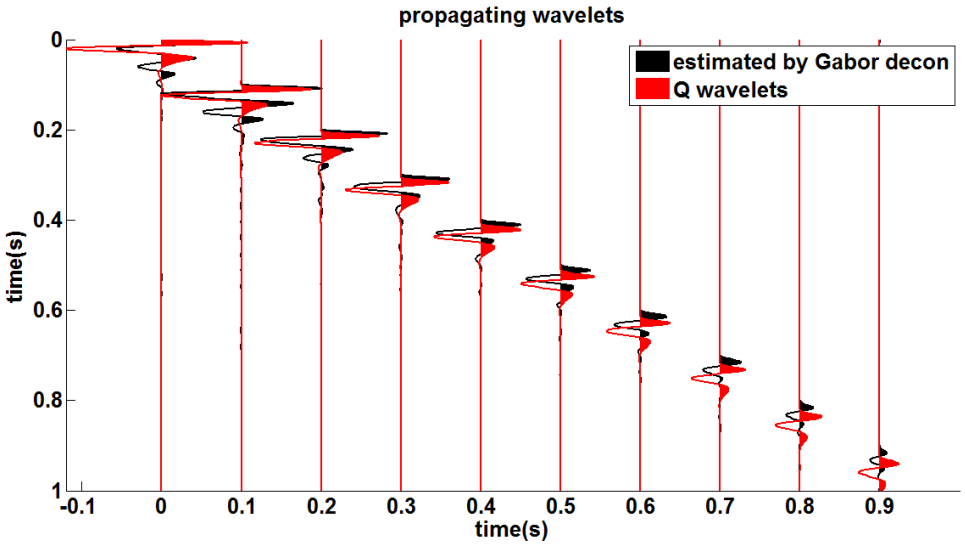

FIG. 8. Comparison of the propagating wavelets estimated by Gabor deconvolution and those modeled by the Q matrix.

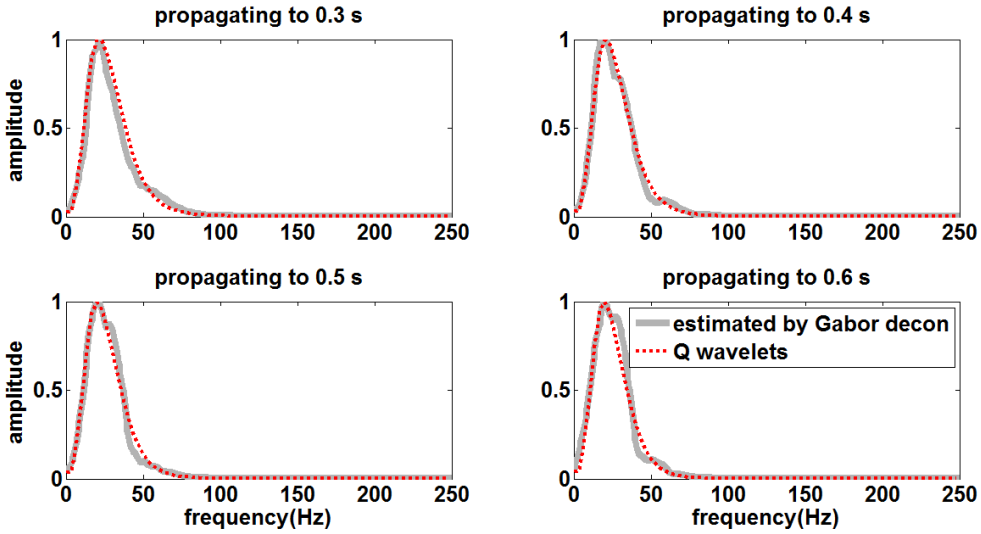

FIG. 9. Amplitude spectra of the wavelets propagating to four different times in Figure 8.

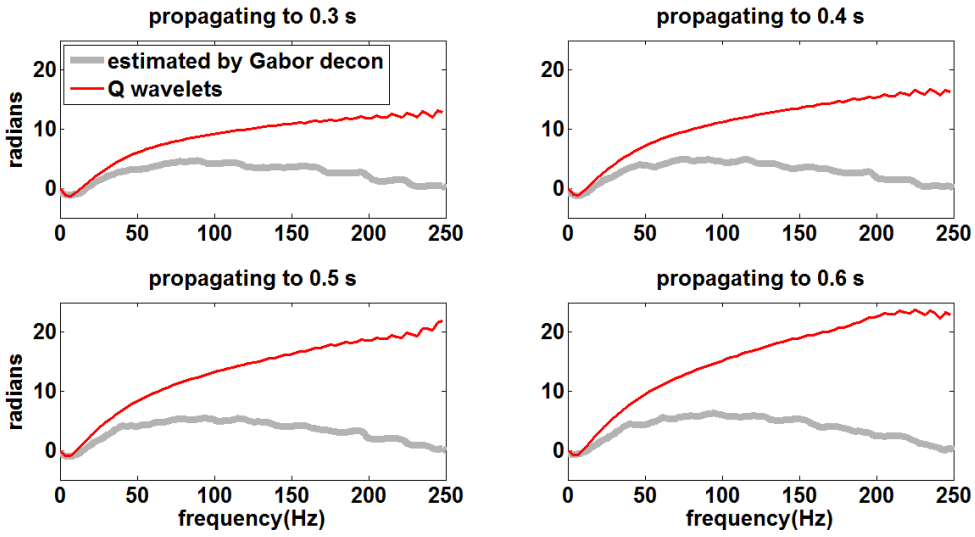

FIG. 10. Phase spectra of the wavelets propagating to four different times in Figure 8.

$$\phi^H_{w_Q}(t,f) = \phi_{w_0}(f) - 2\pi f t(1 - \frac{1}{\pi Q}\ln\frac{f}{f_{NYQ}}) \tag{10}$$

where $\phi^H_{w_Q}(t,f)$ denotes the phase of the propagating wavelet at traveltime t estimated by the digital Hilbert transform. Its phase delay is less than the actual phase at traveltime t with respect to the well logging frequency f_w

$$\phi_{w_Q}(t,f) = \phi_{w_0}(f) - 2\pi f t(1 - \frac{1}{\pi Q}\ln\frac{f}{f_w}). \tag{11}$$

The difference between $\phi_{w_Q}(t,f)$ and $\phi^H_{w_Q}(t,f)$ is the residual phase remaining in the Gabor deconvolved trace compared to the well reflectivity

$$\Delta\phi(t,f) = \phi_{w_Q}(t,f) - \phi^H_{w_Q}(t,f) = \frac{2ft}{Q}\ln\frac{f_{NYQ}}{f_w} \tag{12}$$

where $\Delta\phi(t,f)$ denotes the residual phase and it varies with traveltime t. It can be noticed from Equation 12 that the residual phase at a constant time t is a linear function of frequency f, implying that $\Delta\phi(t,f)$ essentially acts as a time shift operator in the time domain, namely

$$\Delta\phi(t,f) = -2\pi f \Delta drift(t). \tag{13}$$

where $\Delta drift(t)$ is a time-variant time shift function and is called the residual drift time. According to Equations 12 and 13

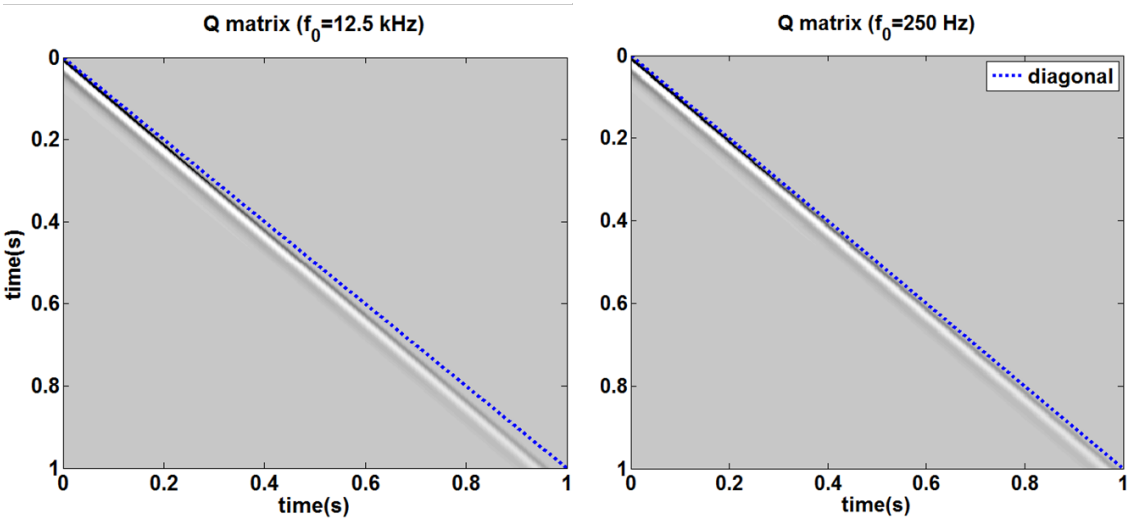

FIG. 11. Comparison of the Q matrixes in gray built using the well logging frequency (left) and the seismic Nyquist frequency (right) as the reference frequency respectively.

$$\Delta drift(t) = \frac{t}{\pi Q} \ln \frac{f_w}{f_{NYQ}}. \tag{14}$$

The residual drift time is the difference between the event time at the seismic Nyquist frequency and at the sonic logging frequency after the difference between the dominant seismic frequency and the Nyquist frequency being removed by Gabor deconvolution. In the case of a time-invariant Q value, $\Delta drift(t)$ is a linear function of t. For a layered medium where the average Q value varies with traveltime, $\Delta drift(t)$ takes on a more complex form.

Figure 11 compares two Q matrixes, of which the only difference is the phases of their Q wavelets. The Q wavelet phases in the left panel are constructed with respect to the well logging frequency (Equation 11), while those in the right panel are with respect to the seismic Nyquist frequency (Equation 10). Although both sets of the Q wavelets lag behind the dashed blue diagonal by a progressively increasing amount, the right-hand set appears less delayed than the left-hand set at the same traveltime. Four Q wavelets propagating to 0.3 s, 0.4 s, 0.5 s and 0.6 s are taken from the Q matrix in Figure 11 right panel and their phase spectra are plotted in dotted black on top of the corresponding panels in Figure 10 to generate Figure 12. The phase spectra of the propagating wavelets estimated by Gabor deconvolution match those of the Q wavelets modeled with respect to the seismic Nyquist frequency. These three sets of wavelets are plotted in the time domain in Figure 13, showing that the propagating wavelets estimated by Gabor deconvolution align those of the Q wavelets modeled with respect to the seismic Nyquist frequency, but are earlier than those modeled with respect to the well logging frequency. Their timing difference at an individual propagating time is a residual drift time and is denoted by a blue brace.

The residual phase can be calculated by Equation 12 as long as the values of Q and f_w are known. Then the phase of the propagating wavelets estimated by Gabor deconvolution

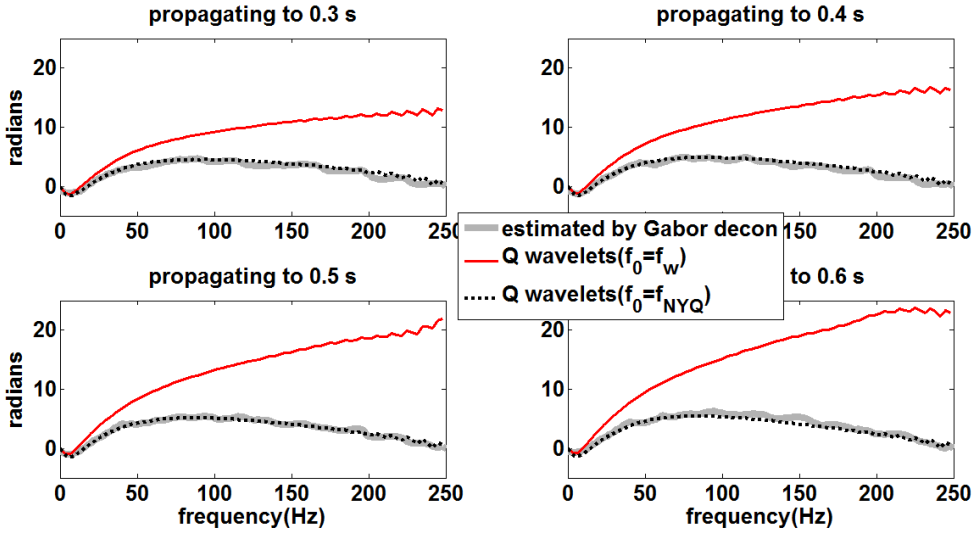

FIG. 12. Same as Figure 10 except that the phase spectra of the propagating wavelets modeled by the Q matrix with respect to the seismic Nyquist frequency are plotted as well.

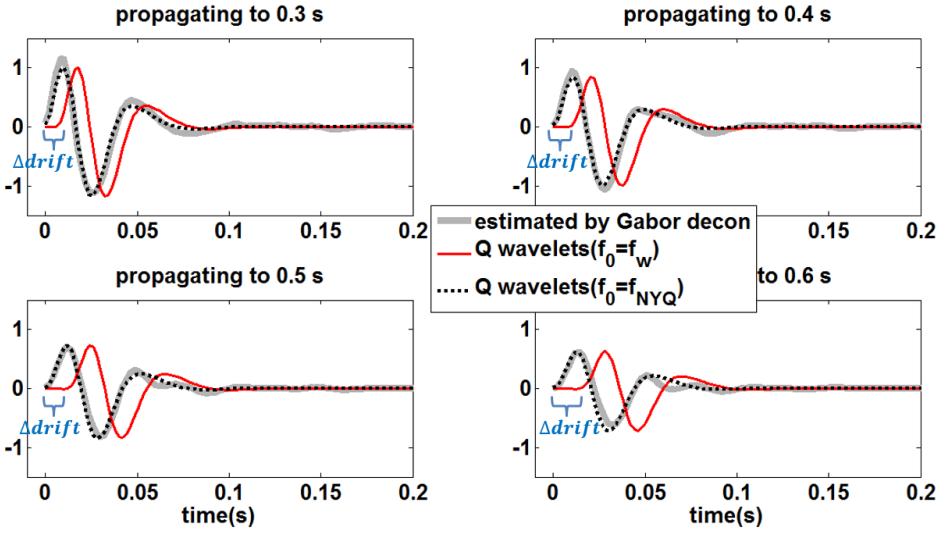

FIG. 13. The time-domain propagating wavelets at four different times estimated by Gabor deconvolution, modeled by the Q matrixes with respect to the well logging frequency and the seismic Nyquist frequency.

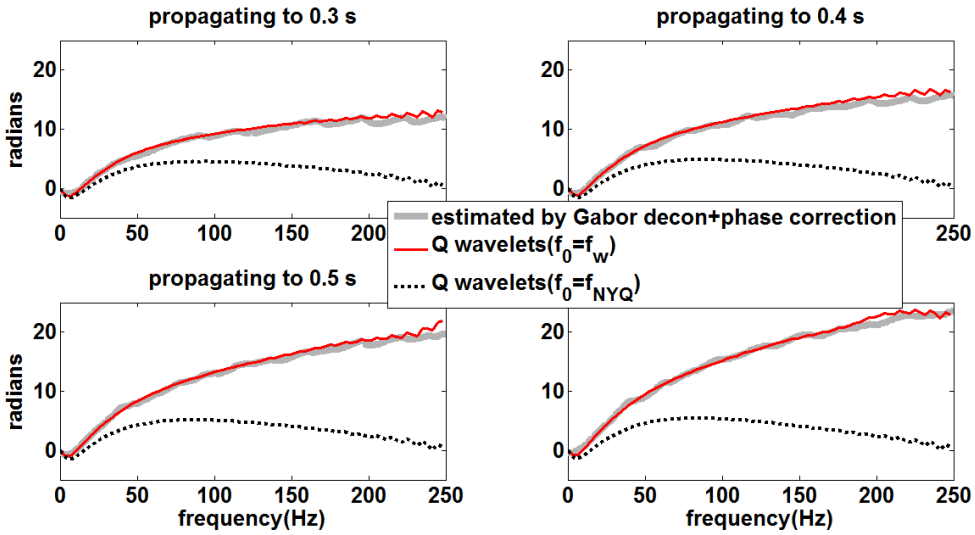

FIG. 14. Same as Figure 12 except that the wavelets estimated by Gabor deconvolution are phase corrected.

can be corrected by

$$\phi^{H,c}_{w_Q}(t,f) = \phi^{H}_{w_Q}(t,f) + \Delta\phi(t,f) \tag{15}$$

where $\phi^{H,c}_{w_Q}(t,f)$ is the corrected phase of the propagating wavelet at traveltime t. With the known values of Q=50 and f_w=12.5 kHz, the phase spectra after correction are calculated and are plotted in bold gray in Figure 14. They are seen to match those of the Q wavelets with respect to the well logging frequency. These three sets of wavelets in Figure 14 are plotted in the time domain in Figure 15, showing that phase correction delays the estimated wavelets by the amount of the corresponding residual drift time to align them with the Q wavelets with respect to the well logging frequency. Similarly, Figure 16 shows the estimated wavelets after phase correction propagating to every 0.1 s in black, the timing of which is consistent with that of the corresponding wavelets embedded in the nonstationary trace in red.

Deconvolving the estimated wavelets with the corrected phases from the nonstationary seismic trace, the estimated reflectivity is shown to be much better tied to the well reflectivity than that without phase correction in Figure 17. Next, the amplitude of the phase corrected reflectivity estimate is balanced and its phase is rotated with respect to the known reflectivity in the same time-variant way as before. It can be observed from Figure 17 that time-variant amplitude balancing and time-variant constant-phase rotation do little change to the phase corrected reflectivity estimate. As a quality control, Figure 18 shows that phase correction reduces both the time-variant constant-phase difference and the time-variant time shift to zero, and enhances the time-variant crosscorrelation coefficient between the estimated and known reflectivities. It can be concluded that running Gabor deconvolution on the nonstationary trace removes the propagating wavelet phase delay to the seismic Nyquist frequency only. By correcting the estimated wavelet phase to the well

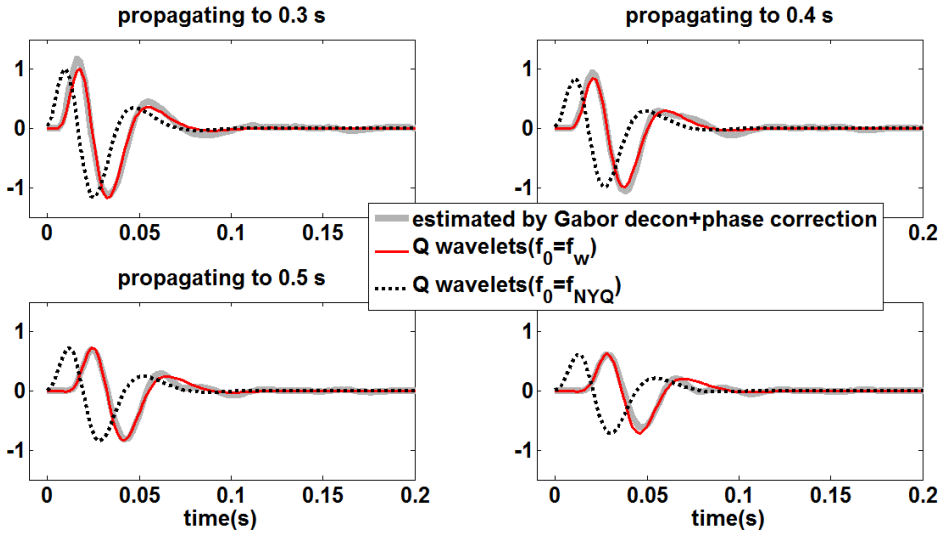

FIG. 15. Same as Figure 13 except that the wavelets estimated by Gabor deconvolution are phase corrected.

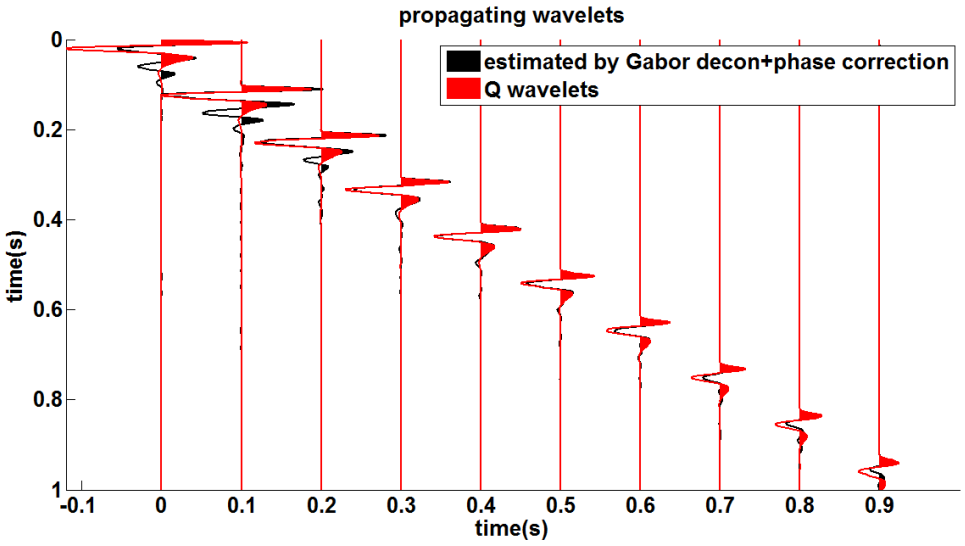

FIG. 16. Comparison of the propagating wavelets estimated by Gabor deconvolution with phase correction and those modeled by the Q matrix with respect to the well logging frequency.

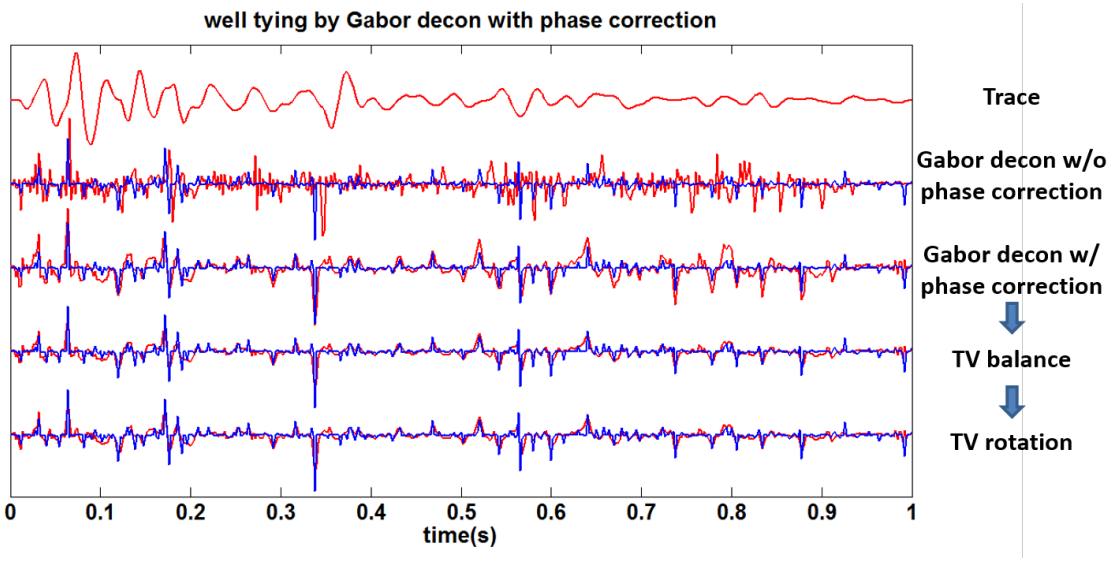

FIG. 17. A procedure of tying the nonstationary trace to the known reflectivity (blue) by Gabor deconvolution, phase correction, time-variant amplitude balancing and time-variant constant-phase rotation.

logging frequency, the Gabor deconvolved trace can be well tied to the known reflectivity with very little amplitude and phase errors.

RESIDUAL DRIFT TIME ESTIMATION AFTER GABOR DECONVOLUTION

As can be seen from Equation 13 that applying phase correction in the Gabor domain is equivalent to applying a time-variant residual drift time correction in the time domain. Figure 19 displays that the Gabor deconvolved trace is precisely tied to the well reflectivity after its timing is corrected by the residual drift time, which is calculated using the known values of Q as well as the well logging frequency via Equation 14 and is plotted in solid gray in Figure 20 top panel. With a time-invariant Q value, the theoretical residual drift time in this case is a linear function of traveltime t.

Although Gabor deconvolution with either phase correction or residual drift time correction can tie the nonstationary seismic trace to the well reflectivity accurately, neither of them works without knowledge of Q or the well logging frequency. Without this information, time-variant crosscorrelation and smooth dynamic time warping (Cui and Margrave, 2014, 2015) are tested to estimate the residual time-variant drift time by matching the Gabor deconvolved seismic trace to the well reflectivity statistically. Figure 20 top panel shows the residual drift time estimated by TVCC in solid blue using a sliding Gaussian window with 200 ms half-width and 10 ms increment, which approximates the known trend but with major discontinuities. The residual drift time estimated by SDTW is plotted in dotted red using a coarse sampling interval h equals 200 samples (namely 0.4 s) and it estimates the known residual drift time perfectly. The timing of the Gabor deconvolved seismic trace is corrected by the estimated residual drift time with each method and is compared to the well reflectivity respectively in Figure 19. It can be observed that the Gabor deconvolved trace corrected by TVCC has obvious misties (indicated by yellow boxes), where the es-

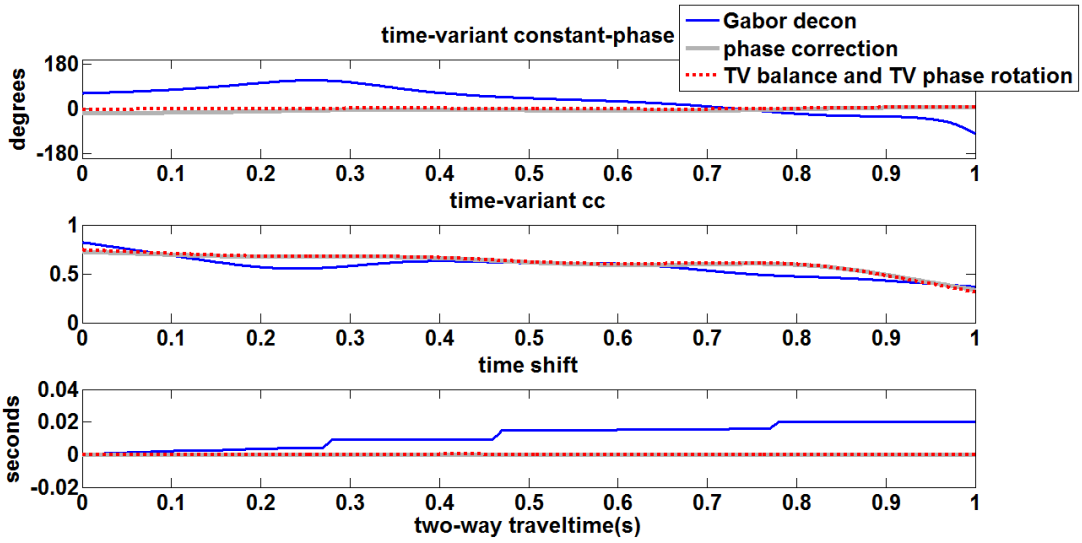

FIG. 18. The time-variant constant-phase differences (top), the time-variant crosscorrelation coefficient sequences (middle) and the time-variant time shift sequences at which the coefficients are obtained (bottom) between the known reflectivity and the Gabor deconvolved trace, the Gabor deconvolved trace after phase correction, the Gabor deconvolved trace after phase correction, time-variant amplitude balancing and time-variant constant-phase rotation.

timated residual drift time has discontinuities. In contrast, the Gabor deconvolved trace corrected by SDTW is well tied to the known reflectivity. As a quality control, the time-variant crosscorrelation coefficient sequences between the well reflectivity and the Gabor deconvolved traces with different residual drift time corrections in Figure 19 are calculated and are plotted in Figure 20 bottom panel, from which we see that the Gabor deconvolved trace corrected by the SDTW estimated residual drift time ties to the well reflectivity as well as that corrected by the known residual drift time and is better than that corrected by the TVCC estimated residual drift time.

CONCLUSIONS

Running Gabor deconvolution on the nonstationary trace can get reflectivity estimate tying the well reflectivity in amplitude and spectral content, but has phase errors which are more complex than those can be solved by time-variant constant-phase rotation. Gabor deconvolution accurately estimates the amplitude spectra of the propagating wavelets. However, it calculates the phase spectra of the propagating wavelets by the digital Hilbert transform, which integrates within the seismic frequency band and corrects the drift time to the Nyquist frequency only.

By correcting the estimated wavelet phase to the well logging frequency, the Gabor deconvolved trace can be well tied to the known reflectivity with very little amplitude and phase errors. Gabor deconvolution with either phase correction or residual drift time correction can tie the nonstationary seismic trace to the well reflectivity accurately knowing the Q values and the well logging frequency. Smooth dynamic time warping can estimate the residual drift time without knowledge of Q or the well logging frequency, and the estimation is more accurate than time-variant crosscorrelation.

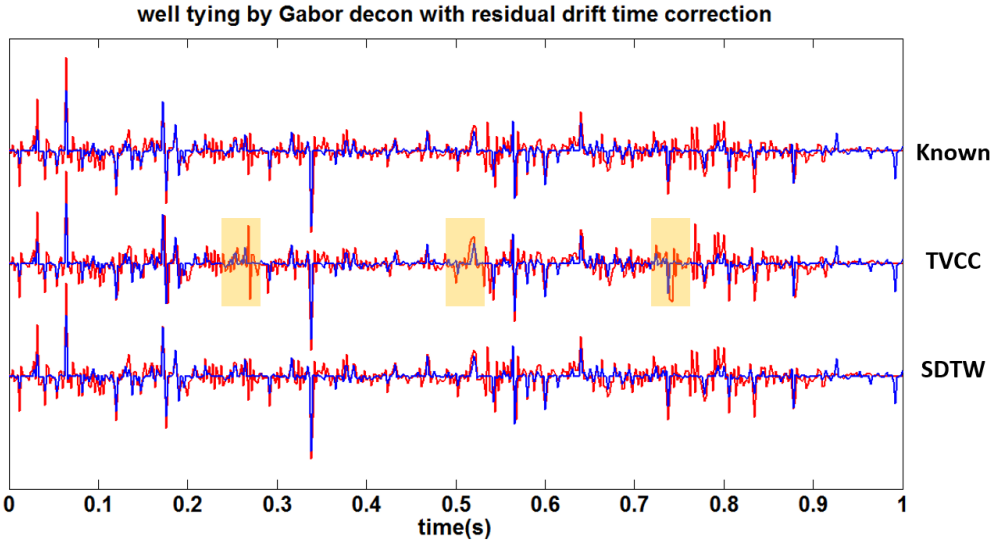

FIG. 19. The Gabor deconvolved trace corrected by the known residual drift time, the residual drift time estimated by time-variant crosscorrelation and the residual drift time estimated by smooth dynamic time warping compared to the well reflectivity (blue) separately.

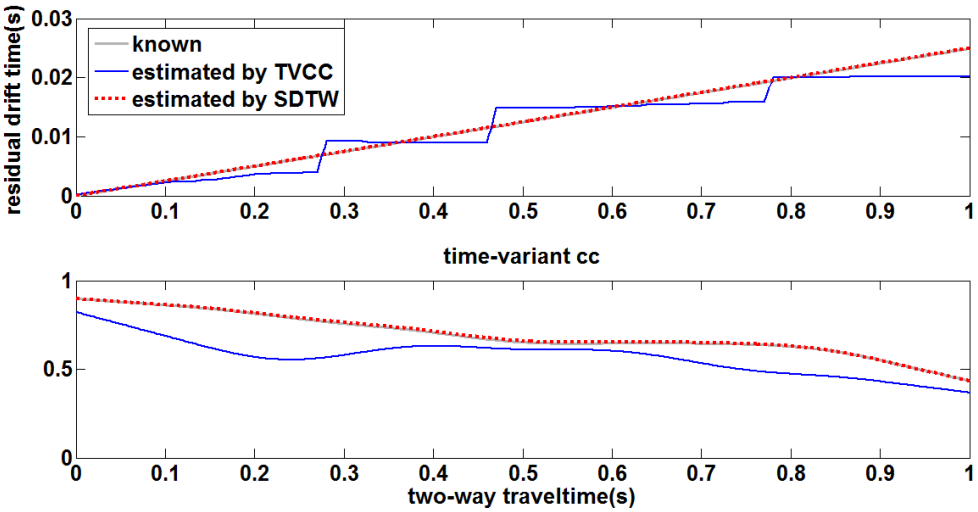

FIG. 20. Residual drift time after Gabor deconvolution: the known function, time-variant crosscorrelation estimate and smooth dynamic time warping estimate (top). Time-variant time shift sequences between the known reflectivity and the Gabor deconvolved trace corrected by the known residual drift time, corrected by the residual drift time estimated by time-variant crosscorrelation and corrected by the residual drift time estimated by smooth dynamic time warping (bottom).

ACKNOWLEDGEMENTS

The authors thank the sponsors of CREWES for continued support. This work was funded by CREWES industrial sponsors and NSERC (Natural Science and Engineering Research Council of Canada) through the grant CRDPJ 461179-13. Author 1 was also supported by scholarships from the SEG Foundation and the Department of Geoscience at the University of Calgary.

REFERENCES

Cui, T., and Margrave, G. F., 2014, Drift time estimation by dynamic time warping: CREWES Research Report, **26**, 17.1–17.20.

Cui, T., and Margrave, G. F., 2015, Seismic-to-well ties by smooth dynamic time warping: CREWES Research Report, **27**.

Margrave, G. F., 1998, Theory of nonstationary linear filtering in the fourier domain with application to time-variant filtering: Geophysics, **63**, 244–259.

Margrave, G. F., 2013, Why seismic-to-well ties are difficult: CREWES Research Report, **25**, 59.1–59.26.

Margrave, G. F., and Lamoureux, M. P., 2001, Gabor deconvolution: CREWES Research Report, **13**, 241–276.

Margrave, G. F., Lamoureux, M. P., and Henley, D. C., 2011, Gabor deconvolution: Estimating reflectivity by nonstationary deconvolution of seismic data: Geophysics, **76**, W15–W30.

Sheriff, R. E., and Geldart, L. P., 1995, Exploration seismology: Cambridge University Press.